HAL open science

Experimental characterisations and numerical simulation of fluid-structure interactions for casting control

Aboubakry Agne, Michel Arrigoni, N. Montagu, Julien Le Clanche, M. Long, Mylène Leduc, Alexandre Charles, Ngadia Tahane Niane, Steven Kerampran

To cite this version:

Aboubakry Agne, Michel Arrigoni, N. Montagu, Julien Le Clanche, M. Long, et al.. Experimental characterisations and numerical simulation of fluid-structure interactions for casting control. 25e Congrès Français de Mécanique, Aug 2022, Nantes, France. hal-04281704

HAL Id: hal-04281704

https://hal.science/hal-04281704v1

Submitted on 14 Nov 2023

HAL is a multi-disciplinary open access archive for the deposit and dissemination of scientific research documents, whether they are published or not. The documents may come from teaching and research institutions in France or abroad, or from public or private research centers.

L'archive ouverte pluridisciplinaire **HAL**, est destinée au dépôt et à la diffusion de documents scientifiques de niveau recherche, publiés ou non, émanant des établissements d'enseignement et de recherche français ou étrangers, des laboratoires publics ou privés.

EXPERIMENTAL CHARACTERIZATIONS AND NUMERICAL SIMULATION OF FLUID-STRUCTURE INTERACTION FOR CASTING CONTROL

A. AGNE[a], M. ARRIGONI[b], N. MONTAGU[a], J. LE CLANCHE[b], M. LONG[a], M. LEDUC[a], A. CHARLES[a], T.N. NIANE[a], S. KERAMPRAN[b]

a. SAFRAN TECH, Plateforme Aubes de Turbines Avancées, 92 700 Colombes, France, aboubakry.agne@safrangroup.com
b. ENSTA Bretagne, IRDL, UMR 6027 CNRS, 29806 Brest, France, michel.arrigoni@ensta-bretagne.fr

Résumé :

Les aubes creuses des étages les plus chaud de turboréacteur sont fabriquées par un procédé de fonderie à cire perdue. Après plusieurs étapes visant à fabriquer un moule consommable avec inserts/noyaux, la phase de fusion ou coulée est une étape clé de la gamme qui consiste à verser un superalliage à base de Nickel à l'état liquide dans le moule puis à le solidifier. En vue d'améliorer le processus de fabrication, notamment l'étape de fusion, l'interaction entre le métal en fusion et les inserts/noyaux de fonderie est étudiée pour plusieurs vitesses d'écoulement représentatives du procédé. Dans le but de mieux comprendre cette interaction difficilement observable lors d'une coulée, nous avons recours à un dialogue essai - calcul.
Des calculs hydrodynamiques sont corrélés et validés à l'aide d'un montage expérimental développé spécifiquement pour cette étude, et dans lequel le métal en fusion est remplacé par de l'eau sur la base d'une similitude en viscosité. Une modélisation du banc d'essais expérimental a été réalisée avec le code de calcul FLOW-3D®, un outil CFD dédié aux mouvements de surfaces libres et disposant d'un module d'interaction fluide-structure. Les résultats des calculs d'écoulement permettent de retrouver les tendances du champ de vitesse dans le fluide autour d'une structure rigide et celles du champ de déplacement d'une structure flexible avec un bon accord avec les observations expérimentales.

Abstract :

Hollow turbojet blades are manufactured by a lost-wax casting process. After several steps aimed at manufacturing a consumable mold with inserts, the pouring or casting phase is a key step in the process, which consists of pouring a nickel-based superalloy at liquid state into the mold and then solidifying it. In order to improve the manufacturing process, chiefly the pouring step, the interaction between the molten metal and the thin walls of the casting mold are studied for several flow rates representative of

the process. In order to better understand this interaction, which is difficult to observe during a casting, we use a test-calculation dialogue.
Hydrodynamic and fluid-structure interaction calculations are correlated and validated using an experimental setup developed specifically for this study, in which molten metal is replaced by water based on Reynolds number similarity. A model of the experimental test bench was carried out with the calculation code FLOW-3D®, a CFD tool dedicated to free surface movements including a fluid-structure model. The results of the flow calculations allow to find the trends of the velocity field in the fluid around the structure and its displacement with a good agreement with the experimental observations.

Keywords: Casting, Fluid-Structure Interaction, experimental fluid mechanics, CFD, manufacturing digital twin.

1 Introduction

Among the many steps of an investment casting process, the pouring step can generate many defects affecting the final quality of the mold part. For example, the melted metal may not completely fill the mold (air entrapment) or impurities may lead to nucleation defects [1]. In addition, the case of a mold containing structures such as foundry cores may exhibit dimensional non-conformities due to the displacement of the cores during and after the interaction with the liquid metal. Therefore, this filling process represents an important field of interest in the industry through several studies focusing on the validation of numerical models with experimental data [2, 3, 4, 5] in order to predict and avoid part defects during the mold filling process.

The present experimental and numerical study is part of a project dealing with a particular mold filling process during metal melting, namely the filling of a cavity with the presence of a core in the casting of a cooled blade with the investment casting process. Cooled blades are typically used in aircraft or helicopter turbines, which are subject to high operating temperatures and provide additional cooling leverage. During the casting process of these cooled blades [6], the mechanical loading induced by the interaction between the core (corresponding to the cooled parts of the blade), the mold and the molten metal can generate deflections or offsets of the core [7]. Consequently, dimensional defects on the final part (non-conformity) or even metal leaks on the mold, are to be observed. Improve the manufacturing of casting molds with cores has to rely on numerical simulation considering the pouring step happens in a Bridgman furnace and can hardly be monitored. The overall scientific approach is, first, to define a relevant fluid-structure interaction (FSI) model, validated by representative experiments; second, to derive from the FSI models a casting numerical twin to adress the robustness of different molding strategy to reduce defects. The present paper focus on the first aspect

Water is used in place of the molten superalloy for the exploration of a FSI model. Indeed, water at ambient temperature and molten metal at casting temperature have a dynamic viscosity in the same order of magnitude (0.001 vs 0.005 Pa.s) [8]. Note that there is a considerable difference in density between water and a molten superalloy. The fluid/structure interaction is classically studied in the naval industry because of the phenomena of slamming and sloshing which can induce important structural damage [9] and the studies associated with this field of interest mainly deal with moving bodies impacting a water

surface initially considered at steady state. The penetration of a shape into water can generate deformations of the water surface [10, 11], which can be characterized by water velocity flow fields that can be observed by particle image velocimetry (PIV) [12], in addition to significant dynamic pressure loads [13, 14] that are mainly due to the geometry of the impacting body [9]. Finally, depending on several parameters such as the geometry of the body, its wettability (characterized by the contact angle) or the impact characteristics (impact velocity), the water entry can be considered in two different forms: hydrophilic with a simple deformation of the water surface or hydrophobic with the formation of an air entraining cavity [8, 11].

The aim of this paper is to characterize the confined water/core interactions using two main measurement techniques in order to validate numerical models in the case of hydraulic impacts with embedded cores. The experimental characterization has required the design of an original setup [15]. A numerical model of the test bench was carried out with the calculation code FLOW-3D®, a CFD tool dedicated to free surface movements, including a fluid-structure interaction module. The results of the flow calculations allow to find the displacement trends of a flexible core, made of Agilus30®, tested in the experimental setup. The flow induced offset of the flexible core was observed during the confined rise of the fluid by using visualization techniques such as shadowgraphy and Schlieren imaging with a high-speed camera. The repeatability of these tests was verified for a given ascending speed and then the evolution of the maximum core deflection as a function of the ascending speed was determined. This configuration was also modeled in FLOW-3D® by integrating the elastic behavior of the soft/flexible core for the deflection calculation. The numerical results fits the experimental ones and lies within the experimental errors, opening encouraging outlooks for the understanding of the fluid-structure interaction during the melting stage.

2 An original set-up to investigate the confined water/core interactions

The experimental setup was designed to generate a vertically rising water surface at a constant velocity U in a square cross-section test section before impacting a rigid or flexible immobile core depending on the study requirements. The upstream air supply pressure P_s is first stabilized by a pressure servo-control system and the pressure in the tank (partially filled with water) P_t is increased linearly. Considering water (density ρ = 1000 kg/m3) as an inviscid fluid [5], the tank pressure ramp $\dot{P}_t$ can be correlated with the upstream velocity U according to the relationship (1):

$$\dot{P}_t = U\rho g\left(1 + \frac{S}{S_t}\right) \qquad (1)$$

Where the water surface in the tank is S_t = 57 x 10^3 mm² and S = 80 x 80 mm² the test section cross section. g is the gravity constant and is 9.81 m/s^{-2}.

The experimental set-up presented in figure 1 consists of a 40 L tank partially filled with water and connected to the 80 x 80 mm² square test section. The test section is made of PMMA panels bonded with a transparent glue to allow the visualization of the flow with a high-speed camera PROMON U750 which can film up to 500 images per second with a resolution of 800 x 600 pix². A converging nozzle is used to adapt the flow from a circular section in the tank to a square section in the flow path. The contraction ratio was estimated at 5.8 by CFD calculation, not detailed here. On order to stabilize the flow, this nozzle was fitted with a honeycomb plate with a 93% cross-sectional area (20 mm wall

thickness), and cell size inscribed in a 10 mm circle and 20 mm in height. The top of the test section is kept open and allows to establish the atmospheric pressure P_{atm} = 1.013 bar inside. The air pressure in the tank is recorded with a frequency of 50 Hz by a Keller PR41X pressure transmitter with an accuracy of 80 Pa. An injection pressure P_s is imposed in the tank and is controlled by a Brooks SLA5800 pressure regulator connected to an IFM PT54 pressure transmitter with an accuracy of 0.5 %. A buffer tank connected to the laboratory's compressed air network and equipped with a pressure reducing valve supplies the air injection in the water tank, this allows to limit the injection pressure oscillations depending on the laboratory's air network variations. The ambient temperature is measured during the experiment with an NTC thermocouple. This temperature is constant and equal to 20°C ± 1. The displacement of the core was measured with an Axom OWLF 4007 FA S1 laser telemetry operating at 1.1 kHz and having an accuracy of 5 µm over a range distance between 30 and 70 mm from the sensor. A strioscopic setup is used in order to visualize the wave fronts and turbulences during the liquid/core interaction (fig. 1). In addition, the liquid is seeded with fine polymer particles of about 30 µm diameter which materialize tracers when illuminated by a laser plane.

The presented experimental set-up allows first to track the flow around an obstacle and second to measure the deflection of a core placed in the flow.

First, reporting to fast imaging, it is possible to track the displacement of flow suspended particles as a function of time. This technique is called Particle Imaging Velocity (PIV) and has been presented in reference [15]. This technique was applied in the case of the flow around a PVC made rigid cylinder with a diameter of 40 mm and a length of 100 mm. Details on this test can be found in [15].

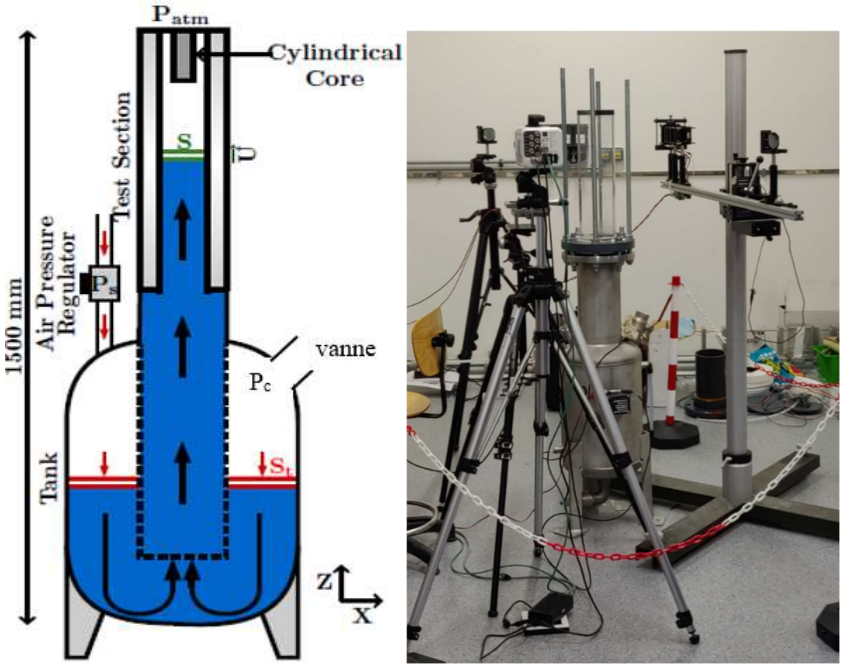

Figure 1: Schematic view of the experimental setup and strioscopic setup around the test bench.

Second, laser telemetry was applied to monitor the core displacement/offset study of an Agilus30® resin core fixed to the upper extremity of the test section. This material has properties to undergo large deformations in repeated torsion and bending. Its Shore A hardness is 30. The specimen is beveled at 45° at its lower end in order to accentuate the offset of the non-beveled side during the interaction with

the rising liquid. The test sample is attached by a cylindrical fitting 40 mm high and 40 mm in diameter, keyed to prevent rotation. A length of 100 mm is presented in the form of a wing of oval section of large axis 40 mm and small axis 10 mm (fig. 2). This core is subjected to liquid impact velocities of 0.15 m/s; 0.20 m/s; 0.25 m/s; 0.30 m/s; 0.4 m/s; 0.5 m/s; 0.6 m/s; 0.7 m/s; 0.8 m/s; 0.9 m/s and 1 m/s. For each speed, 5 tests are carried out in order to check the repeatability and the standard deviations of the tests. From 0.5 m/s, the acquisition frequency of the fast camera is doubled from 1 kHz to 2 kHz for a better accuracy. The deflection measure with the Axom OWLF 4007 telemeter is non intrusive (figure 3), the measure uncertainty is between 0.004mm and 0.02 mm with an acquisition precision of 0.0049 mm. The centerline of the specimen at the stagnation point stands for the spatial origin in the rest of the paper. During an experiment, the so called measured core deflection refers to the difference between the maximum distance over time measured by the telemeter and the minimum one. Note that the direction of deflection is forced by the bevel.

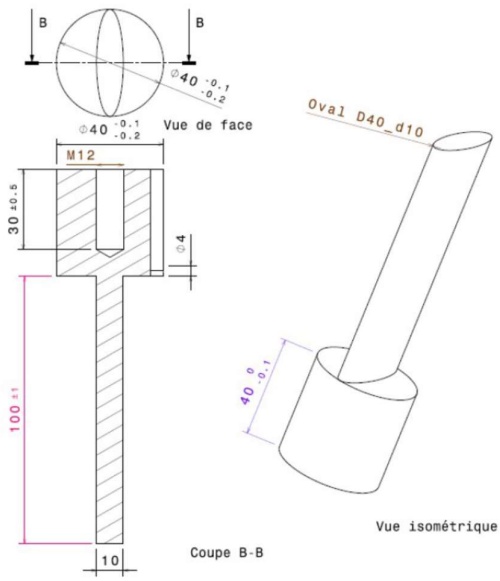

Figure 2: Definition drawings of the bevelled core in Agilus30®.

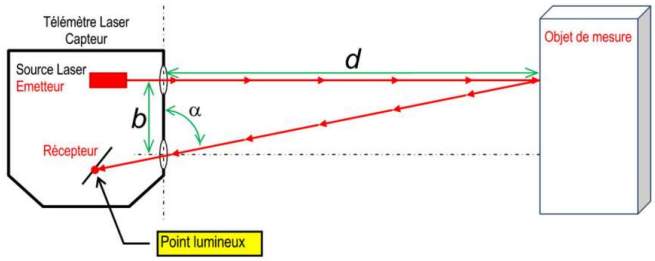

Figure 3 : Scheme of distance measurement by triangulation, from bullier automation® [18].

3 Numerical modelling of the confined water/core interactions

Numerical modelling of the confined water flow

Only the "useful" area of the experimental set-up is meshed (see figure 4) whereas an imposed input velocity models the pressurized tank and the lower part of the flow path. This way of modelling somehow assumes the experimental set-up is perfect in generating a homogeneous non-turbulent flow in the flow path. The imposed velocity at the bottom of the useful area comes from experimental measure whereas atmospheric pressure is imposed at the top the domain. In spite of the symmetry of the integration domain, no symmetric conditions are imposed in order to allow the core displacement solution to deflect. The domain is made by a one meter long of the flow path with a core in Agilus®.

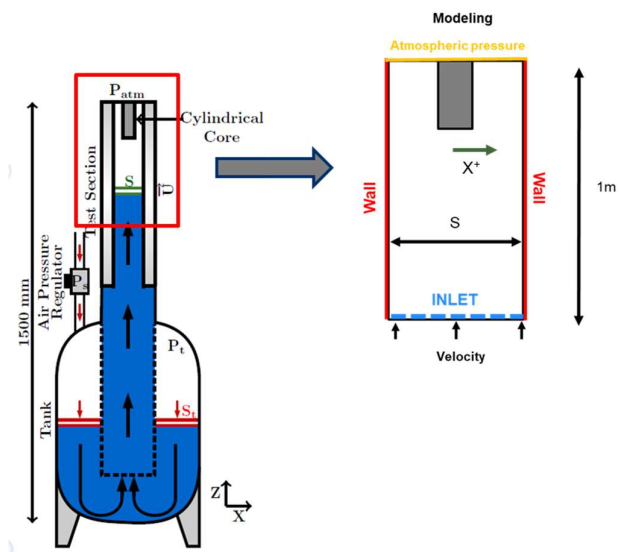

Figure 4 : Numerical modeling of the confined water/core interactions set-up

Flow turbulence is characterized by the Reynolds number (2). Given the viscosity of water (table 1) and the length of the set-up, the flow in the flow path becomes turbulent (Re >> 2 000) for the lowest velocity tested (0.15 m/s):

$$R_e = \frac{VL_c}{\nu} \tag{2}$$

where V is the fluid velocity (m/s), L_c the characteristic length (in our case, the test area length ~1m) and ν the kinematic viscosity (m²/s).

However, even in the case where the flow is steady upstream from the core, the flow may become turbulent as the front of fluid impact the core. Accordingly, the numerical model presented hereafter accounts for turbulence modelling. More precisely, we used a *k-ω* model that fits for turbulent monophasic flows [16].

Density (kg/m^3)	1000
Kinematic viscosity (m²/s)	10^{-6}
Superficial tension (N/m)	7,28 x 10^{-2}

Table 1: Thermo-physical properties of water 20°C.

The convergence of the numerical solution with respect to the finite volume mesh of the flow domain has been studied but won't be detailed here. In a nutshell, the main criterium for this study is the y^+ factor. In fluid mechanics, y^+ denotes the dimensionless wall distance [17]:

$$y^+ = \frac{y\,\rho_f\,u_T}{\mu} \tag{3}$$

Where u_T denotes the shear velocity in the vicinity of the wall, μ the dynamic viscosity of the fluid, ρ_f the density and finally y denotes the distance to the nearest wall, intrinsically corresponding to the cell size at the wall.
By choosing a value for y corresponding to the mesh size, we turn the adimensionnal distance to the wall into a criterium on the mesh that measures the ability of the cells in the mesh to catch the boundary layer near the wall. Depending on the wall treatment of the chosen turbulence model, y^+ values must usually be comprised between 30 and 100, (up to 500 at most), in order to provide a smooth transition between the viscous sublayer and the turbulent region [16, 17]. This criterium is an a posteriori criterium, given the solution in velocity is needed to compute y^+ in most practical cases.

The output of the iterative optimization of the mesh with respect to y^+ is an heterogenous mesh of 130 000 cells, with smaller cells size near the wall and the core. The mesh alleviate the computation time (2h on 10 CPUs) while respecting the y+ criterion.

Mechanical modelling of the Agilus® made supple core

The core made in Agilus® 30 is modelled as a linear elastic solid. The elastic properties used in simulation comes from literature [19] and are to be found on table 2. From a numerical point of view, the core is discretized as a finite element domain in Flow3-D® made of 112 539 order-1 tetra elements.

The core is embedded on its basis, the remaining core boundaries are subject to fluid-structure interaction with the confined flow. This boundary condition is solved by the fluid-structure interaction module of Flow3-D®. The module solves the continuity at the interface between the stress in the body, discretized as a finite element tensor field, and the shear and pressure forces in the flow, discretized with finite volumes [16].

Properties	*Values*
Density ρ	1140 kg.m^{-3}
Young Modulus E	3,25 MPa
Poisson coefficient ν	0,45

Table 2: Elastic properties used in simulation for Agilus® [19].

4 Experimental measure of the core deflection

The camera snapshot presented on fig. 5 shows a turbulent flow, even in the case of the lower velocities. In addition, for a range of velocities between 0,15 m/s and 0,25 m/s upstream from the core, the shape of the flow around the core remains the same. At first, the symmetry of the flow front is broken as the front reaches the bevel of the core. Eddies then appear at the core edges. These eddies are no surprise but they settle quiet slowly: they appear 140 ms after the initial impact on the flat side and after 400 ms on the lateral edges. One can observe a single boundary layer that follow the eddies.

At first, the impact is not symmetrical because of the bevel on the right side of the core. Then, the vortices settle at the two edges of the core. These vortices are quite long to set up compared to the kinematics of the impact. At 140 ms after the impact, the vortex on the flat side appears, after 400 ms, they are established on each side of the core. The formation of a boundary layer is visible and goes up along the generators of the core. On all the photos taken in strioscopy, the real diameter of the visualized disk is the same as the one of the mirrors used, i.e. 5.08 cm.
These vortices can create lift according to $\vec{x}$ in a manner similar to the Vortex Induced Oscillations (VIOs) generated by von Karman vortices on a cylinder. This phenomenon is observed in some core offset measurements where the oscillation is visible. Figure 6 shows a peak at the frequency of appearance of the vortices, namely one every 0.9 seconds. The core is not symmetrical and tends to move closer to the wall, despite the vortices that periodically move it away.

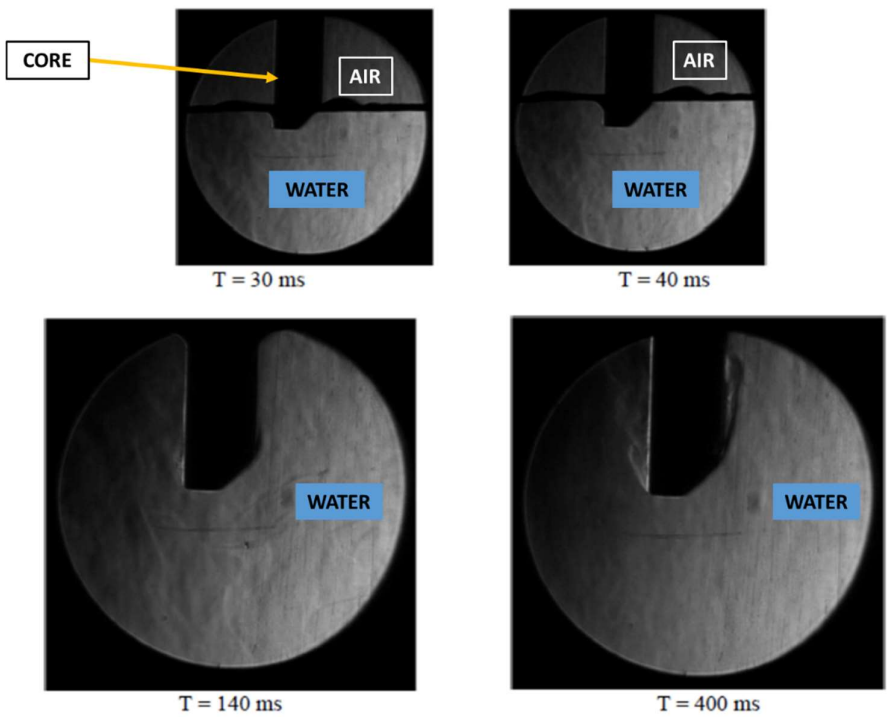

Figure 5 : Pictures from strioscopy observation of the liquid / core interaction at U=0.14 m/s.

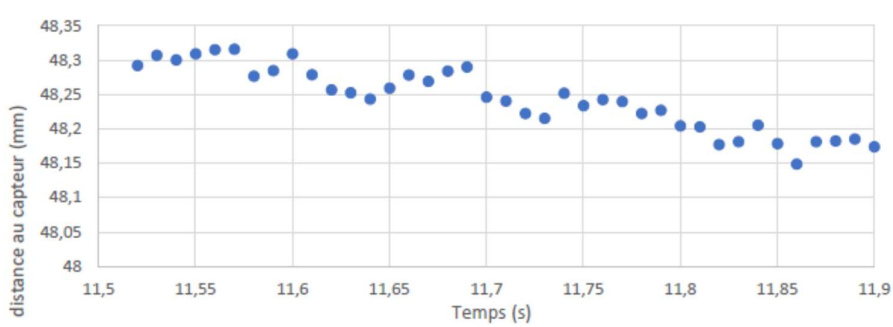

Figure 6: measurement of the displacement of the core after the impact of water at U = 0.14 m/s carried out with the laser rangefinder OWLF 4007 in the 80 x 80 mm² flow path.

At U = 0.30 m/s, the flow changes significantly. Indeed, on the flat side of the core, the vortices are replaced by a small recirculation zone that sets up in time (Fig. 7). On the beveled side, the vortex is still in place. At this velocity, the free surface is deformed at impact, but this phenomenon does not seem to quantifiably disturb the offset measurements. Moreover, the free surface restabilizes after the impact.

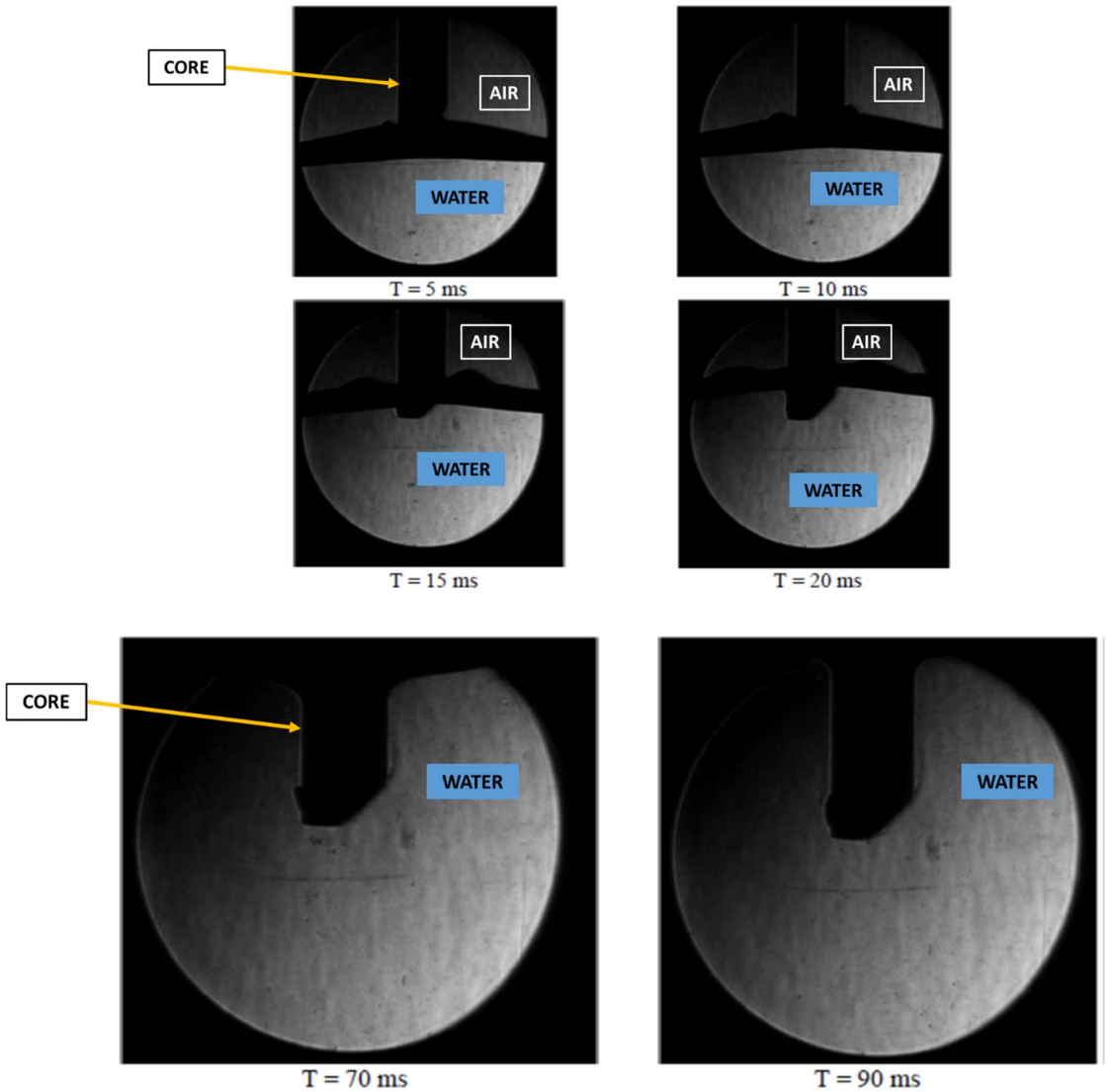

Figure 7: Strioscopic view of the flow around the Agilus® core at U = 0,32 m/s.

For velocities from 0.40 m/s to 1 m/s, the flow appears to be structured in the same way, and the impact is increasingly powerful. This time, recirculation is established on both sides of the core (Fig. 8). Moreover, we notice the appearance of a recirculation zone at the top of the core. This does not appear on every trial, but randomly about once in two. There is no obvious parameter to explain the existence of this recirculation. It probably comes from an asperity in the core which gives rise to it. For speeds of 1 m/s, the free surface remains sufficiently flat before impact to conduct the tests. However, many bubbles appear in the flow. Given the impact velocity, it is unlikely that the bubbles impacting the core

will significantly modify the offset and the behavior of the core at this velocity. The structure of the flow is not fundamentally altered, and the recirculation zone oscillates slightly over time (Fig. 9).

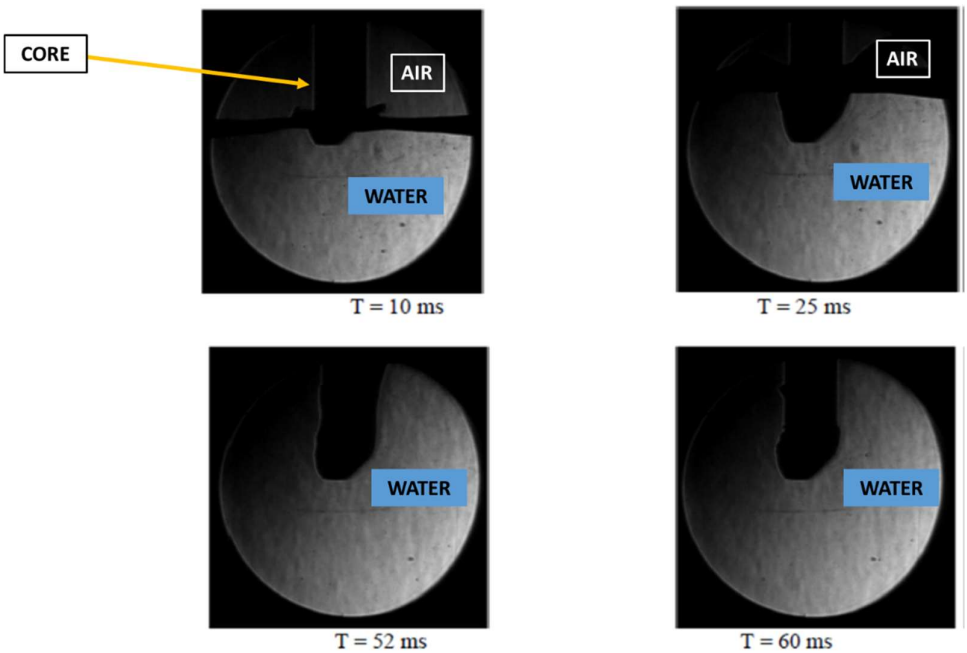

Figure 8: Strioscopic view of the flow around the Agilus® core at U = 0,41 m/s.

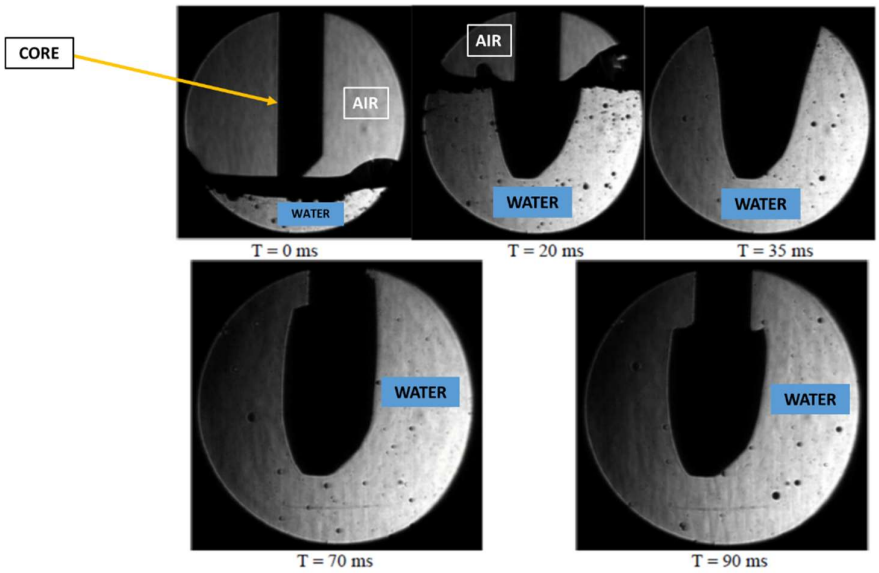

Figure 9: Strioscopic view of the flow around the Agilus® core at U = 0,99 m/s.

Figure 10 is obtained from five offset measurements made for each velocity. Error bars represent the standard deviation of the five measurements of offset *d* and impact speed. A power law trend curve allows the fitting of experimental data (2):

$$d = 3.47\ U^{1.613} \qquad (2)$$

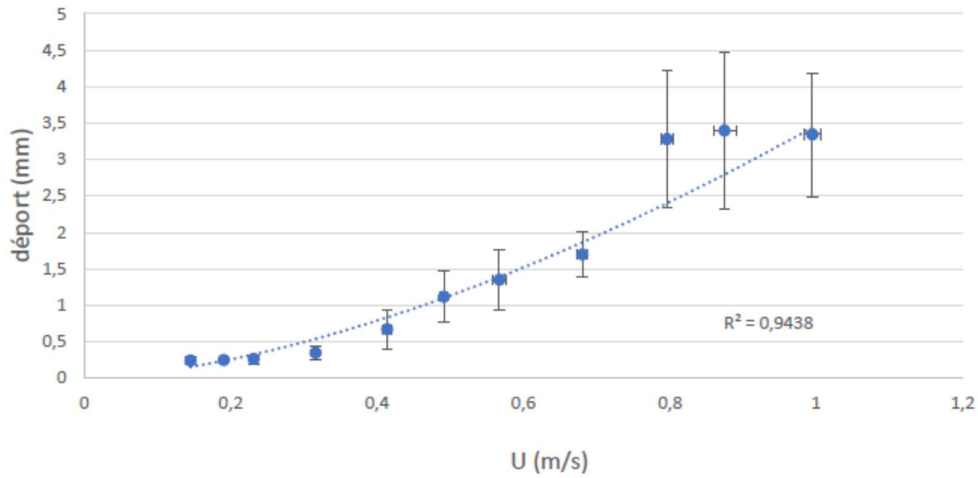

Figure 10: Averaged measurement performed with OWLF 4007 displacement sensor, of the core deflection in Agilus® in test section of 80 x 80 mm².

5 Validation of the pouring numerical model with core deflection experiments

The present section deals with the validation of the numerical model by benchmarking the numerical results with respect to experimental observations. We have a staggered strategy: webench, in a first step, the modelling of the flow only; in a second step, the fluid structure interaction in the case of supple core placed in a confined water flow. Regarding the first purpose, we compare flow velocities snapshots. Regarding the second, we compare numerical predictions and experimental measures of core deflection for a range of inflow velocities.

Snapshots of the experimental the velocity field in the fluid, obtained by PIV measures [15], provide the vertical and radial components of velocities, before, during and after the impact with rigid core. In view of benching numerical model with experimental observations, we compare the vertical velocity (w*) and the radial velocity (u*) 100ms and 200ms after impact (figure 11). An increase in vertical velocity is observed 100 ms after impact, caused by a section reduction. This same phenomenon is encountered in simulation but is underestimated by a third. Radial velocities match between experiments and simulation. After 200 ms, more than a half of the core is immerged. Steady air bubble on the core surface induce disturbance in the velocity field that can be observed on the PIV snapshots.

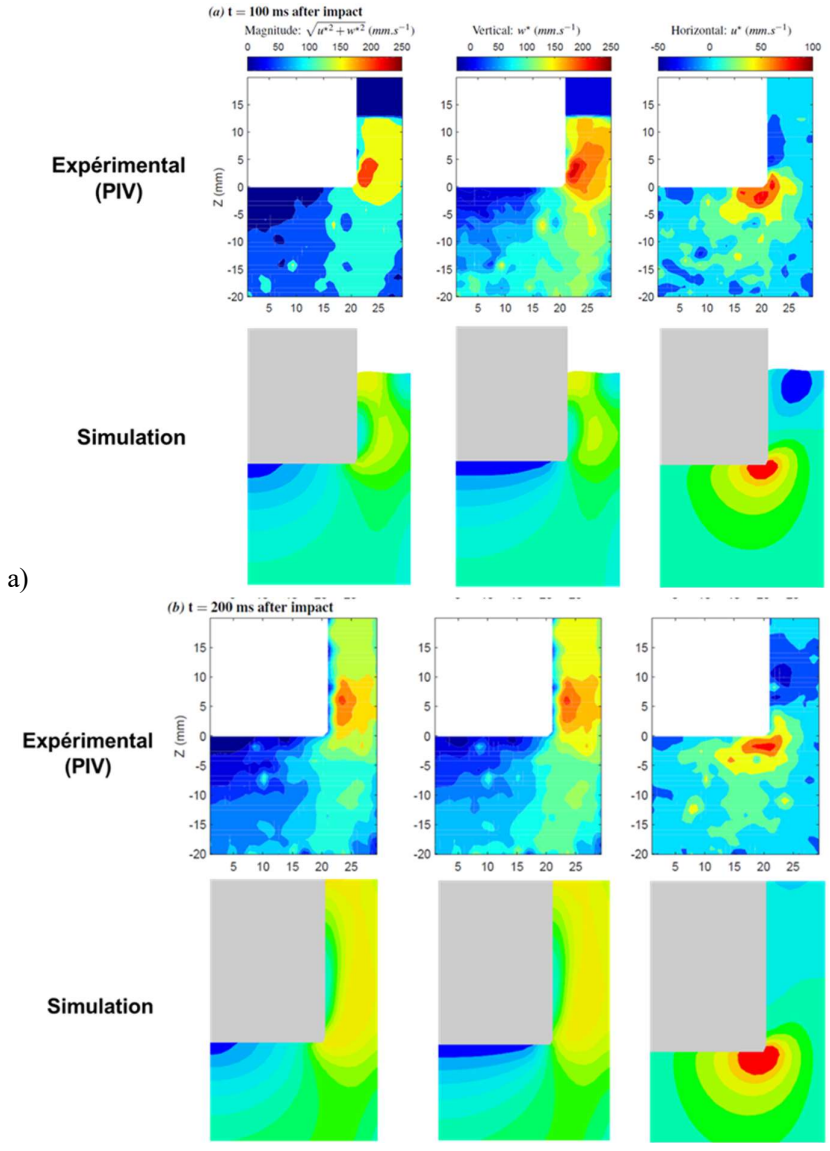

Figure 1: Experimental velocities (PIV) and numerical ones, after impact : a) 100ms after impact and b) 200ms after impact.

We then address the validation of core deflection simulations and compare the experimental deflections (figure 10) with the simulated ones. The deflection has to be computed by taking the difference between the minimum and the maximum position of the core along the deflection axe (depicted as X+ on fig. 4). Figure 13 shows the value of experimental and simulated deflection for different velocities. On the experimental side, 11 points are plotted, each corresponding to the average of 5 measures. Figure 13 also includes information about the variability of the experimental measurements.

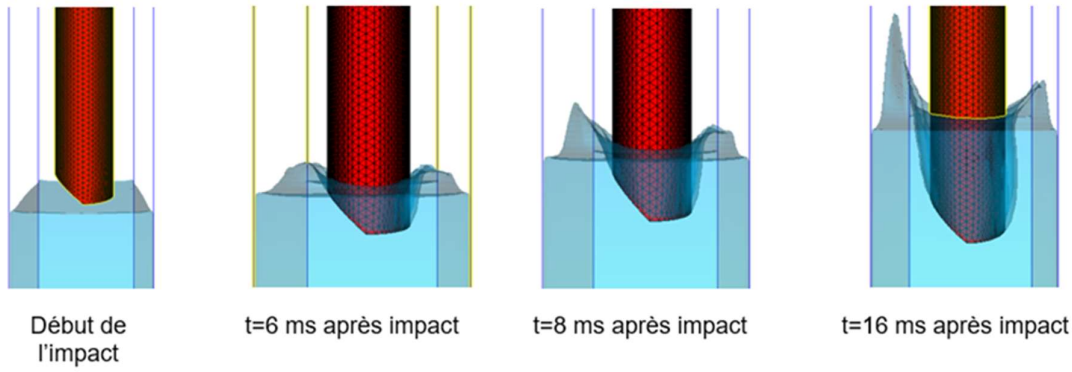

Figure 12: Shape of the free surface impacting the core, inflow velocity being equal to 0,8 m/s.

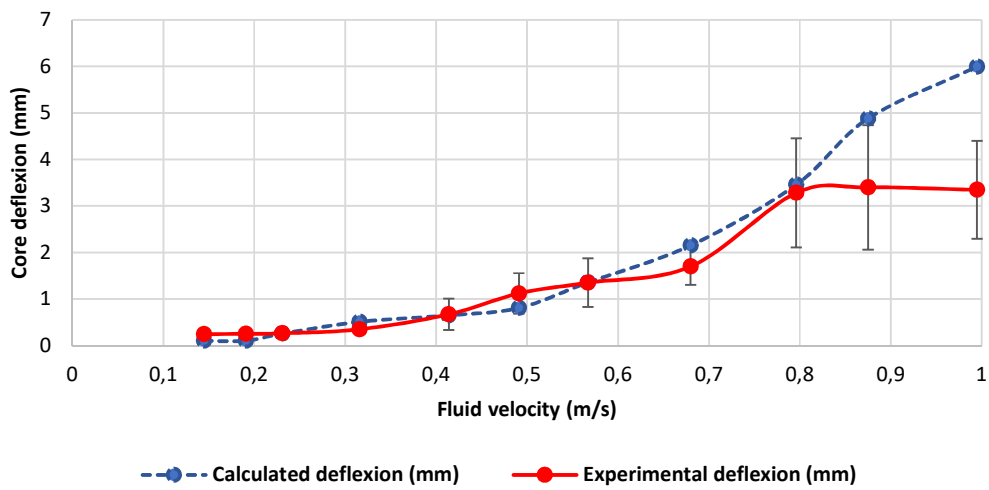

Figure 13: Numerical and experimental core deflection as a function of the velocity, the case of Agilus® made core.

Between 0,1 m/s and 0,8 m/s, the simulated curve fits the experimental one in terms of values and trends (Figure 13). The discrepancy lies within the experimental scatter, even for low velocities (v > 2,5 m/s).

The situation is less clear beyond 0,8 m/s. On the one hand, a significant divergence between experimental and simulated curves has to be reported. Experimentally, the deflection curve stalls whereas the deflection curve is increasing in simulation. On the other hand, the experimental scatter is very high, up to 30 % of the mean value, in the case of higher velocities and the divergence of the curves is not significantly higher that the experimental scatter.

In simulation, the core has been modelled by a linear elastic solid. In practice, material or geometrical non-linearities may arise in the case of large deflection, increasing the overall stiffness of the structure and slowing down the slope of the curve for high velocities. This hypothesis may be tested by injecting the *Flow-3D*® solution in deflection in a structural mechanics solver.

Conclusion

An experimental set-up has been proposed and optimised to assess the core deflection of a supple Agilus® specimen in a 80 x 80 mm^2 confined flow. Experiments were conducted with velocities up to 1 m/s: these experiments were repeatable, at least for velocities up to 0,4 m/s. At lower velocities, eddies induce an oscillation of the core after the initial shock. At higher velocities, air bubbles settle on the side of the core. These bubbles interfere with the telemeter and hamper the quality of the measurement. Nevertheless, we are able to conclude that the core deflection evolves with velocity according to a power law, at least for velocities lower than 0,8 m/s.

In the case of higher velocities, the experimental deflection stalls around 3,5 mm (figure 10). However, this observation is hardly a conclusion since the experimental scatter reaches a third of the value of deflection. The scatter in deflection measures may be related to recirculation area that affects the telemetry process. Another ground of scatter may be the scatter in initial condition, more precisely in the shape of the free surface at the instant of impact. Despite a set-up designed to produce a flow as homogenous and laminar as possible at the entry of the vein, the shape of the free surface is unsteady when it reaches the core, a fact confirmed by simulation when the velocity is higher than 0,8 m/s. The second ground is a key concern in view of the final industrial application. Indeed, we cannot expect the free surface to be flat and repeatable when pouring an industrial mould.

Beside the intrinsic interest of the experiments, they have also been used to evaluate a numerical model based on Flow-3D® that will ultimately help to optimise the pouring of super alloys and improve the casting process of cooled blades. Good fit between experimental observations and numerical results have been reported in terms of distribution of velocity and deflection as a function of the input flow velocity for low and medium velocity.

An additional experimental effort is required to alleviate the remaining uncertainty on the dependence of the deflection on velocities. Suitable modifications of the set-up are currently under discussion in order to address a range of velocity above 1 m/s and to examine the effect of constitutive parameters such as viscosity and density on the deflection.

Acknowledgement

The authors would like to thank Kilian Croci and Vincent Podeur from ENSTA Bretagne and Aymeric Palut from Ecole de l'Air for their contribution to the study as well as Frédéric Montel from ENSTA Bretagne for the programming of the pressure servo-control system.

Références

[1] G. Bellanger, Remplissage des pièces moulées en sable. Système d'attaque. Ed. Techniques Ingénieur, 2006.
[2] Y. Liu, S. Bakhtiyarov, and R. Overfelt, "Numerical modeling and experimental verification of mold filling and evolved gas pressure in lost foam casting process," Journal of Materials science, vol. 37, no. 14, pp. 2997–3003, 2002.
[3] S.-G. Liu, F.-Y. Cao, X.-Y. Zhao, Y.-D. Jia, Z.-L. Ning, and J.-F. Sun, "Characteristics of mold filling and entrainment of oxide film in low pressure casting of a356 alloy," Materials Science and Engineering: A, vol. 626, pp. 159 – 164, 2015.

[4] A. Viswanath, M. Manu, S. Savithri, and U. Pillai, "Numerical simulation and experimental validation of free surface flows during low pressure casting process," Journal of Materials Processing Technology, vol. 244, pp. 320 – 330, 2017.
[5] A. Sanitas, M. Bedel, and M. El Mansori, "Experimental and numerical study of section restriction effects on filling behavior in low-pressure aluminum casting," Journal of Materials Processing Technology, vol. 254, pp. 124 – 134, 2018.
[6] H. Wu, D. Li, and N. Guo, "Fabrication of integral ceramic mold for investment casting of hollow turbine blade based on stereolithography," Rapid Prototyping Journal, vol. 15, no. 4, pp. 232–237, 2009. 9
[7] D. Wang, J. Sun, A. Dong, G. Zhu, S. Liu, H. Huang, and D. Shu, "Prediction of core deflection in wax injection for investment casting by using svm and bpnn," The International Journal of Advanced Manufacturing Technology, vol. 101, no. 5-8, pp. 2165–2173, 2019.
[8] T. Truscott, B. Epps, and J. Belden, "Water entry of projectiles," Annual review of fluid mechanics, vol. 46, pp. 355–378, 2014.
[9] A. E. M. Alaoui, A. Nême, A. Tassin, and N. Jacques, "Experimental study of coefficients during vertical water entry of axisymmetric rigid shapes at constant speeds," Applied Ocean Research, vol. 37, pp. 183–197, 2012.
[10] J. Aristoff, T. Truscott, A. Techet, and J. Bush, "The water entry of decelerating spheres," Physics of Fluids, vol. 22, no. 3, p. 032102, 2010.
[11] C. Duez, C. Ybert, C. Clanet, and L. Bocquet, "Making a splash with water repellency," Nature physics, vol. 3, no. 3, p. 180, 2007.
[12] M. Jalalisendi, A. Shams, R. Panciroli, and M. Porfiri, "Experimental reconstruction of three-dimensional hydrodynamic loading in water entry problems through particle image velocimetry," Experiments in Fluids, vol. 56, no. 2, p. 41, 2015.
[13] G. De Backer, M. Vantorre, C. Beels, J. De Pr´e, S. Victor, J. De Rouck, C. Blommaert, and W. Van Paepegem, "Experimental investigation of water impact on axisymmetric bodies," Applied Ocean Research, vol. 31, no. 3, pp. 143–156, 2009.
[14] B. Peseux, L. Gornet, and B. Donguy, "Hydrodynamic impact: numerical and experimental investigations," Journal of Fluids and Structures, vol. 21, no. 3, pp. 277–303, 2005.
[15] Croci, K., Podeur, V., Arrigoni, M., Kerampran, S., Long, M., & Niane, N. (2020, November). Investigation of a rising water surface impacting a motionless cylindrical core in a confined environment within PIV and PVDF gauge measurements. In 17ème Journées de l'Hydrodynamique.
[16] FLOW-3D® Users Manual (2022). FLOW-3D [Computer software]. Santa Fe, NM: Flow Science, Inc. https://www.flow3d.com.
[17] Schlichting (Deceased), H., Gersten, K. (2017). "Boundary–Layer Equations in Plane Flow", "Plate Boundary Layer", Boundary-Layer Theory. Springer, Berlin, Heidelberg. https://doi.org/10.1007/978-3-662-52919-5_6
[18] Sous-lieutenant Aymeric Palut, "Etude du déport noyau", Mémoire de stage de fin d'études, ENSTA Bretagne, 2021.
[19] David M.J. Dykstra, Joris Busink, Bernard Ennis, Corentin Coulais, « Viscoelastic Metamaterials », J. Appl. Mech. 2019, 86(11): 111012.